ADAPTIVE OPTIMAL CONTROL OF ELASTOPLASTIC CONTACT PROBLEMS

THOMAS BETZ, CHRISTIAN MEYER, ANDREAS RADEMACHER, AND KORINNA ROSIN

Abstract. In this article, the optimal control of static elasto-plastic contact problems are discussed. We present regularization approaches for the nondifferentiabilities arising from contact as well as from elastoplasticity in order to apply fast Newton-type solution algorithms. To achieve an efficient algorithm, we adaptively balance the both regularization, the discretization, and the numerical error based on a posteriori error estimates of the different errors. Numerical examples show the efficiency of the presented approach.

Acknowledgements The authors gratefully acknowledge the support given by the DFG in the collaborative research center (SFB) 708 "3D-Surface Engineering für Werkzeugsysteme der Blechumformteilefertigung - Erzeugung, Modellierung, Bearbeitung" in the subproject B8.

1 Introduction

The research presented in this article is motivated by the investigation of a rolling process to structure the surface of a deep drawing tool coated by means of thermal spraying, c.f. [11]. The modelling of this process includes large deformations, elasto-plastic material behaviour, and frictional contact. Each of these phenomena is frequently modeled by a variational inequality (VI). With this paper we lay the foundations for optimizing such rolling processes.

From the viewpoint of optimization and optimal control, respectively, VIs represent a particular challenge, since the solution operator associated with VIs is in general not differentiable, cf. e.g. [17] for the obstacle problem or [7] for the case of static elasto-plasticity. To cope with this challenge, we start our investigation with a simplified static model accounting for a small deformation elasto-plastic material law including linear kinematic hardening and geometrical contact. The model consists of two coupled VIs and thus still covers the main difficulty from an optimization perspective. The volume load serves as control variable, and to simplify the description we assume that no further control or state constraints are present except for the state system. All in all, we obtain an optimal control problem governed by two coupled VIs.

As the control-to-state operator associated with VIs is in general not differentiable, fast gradient-based optimization methods cannot be applied directly. Consequently, various regularization approaches have been introduced to make such problems amenable to fast optimization methods. We only refer to [2, 5, 12–15, 19] and the references therein. A regularization specially tailored to problems of static elastoplasticity has been developed and studied in [10]. We will employ the same method here in combination with a penalty-type regularization for the contact conditions. Our overall regularization is therefore two-fold. The optimization of a model accounting for both effects, i.e., static elastoplasticity and geometric contact, at the same time is a genuine aspect which has not been investigated in the field of optimal control before.

To obtain an efficient optimization algorithm, it is indispensable to adaptively attune the discretization to the regularization. To achieve this balancing of discretization and regularization error, one needs suitable estimators for both error contributions. While the discretization error for the regularized problems is estimated by means of the dual weighted residual (DWR) method, see e.g. [1, 3, 4], we use an extrapolation technique based on two consecutive computations for the regularization error. In [16] a similar approach has successfully been used to optimally control the obstacle problem.

2 Static elastoplasticity with Signorigni contact conditions in 3D

We consider the static model of infinitesimal elastoplasticity under linear kinematic hardening combined with Signorini contact conditions. This model is represented by the following two coupled variational inequalities of the first kind: Find $\boldsymbol{\Sigma} \in S^2$ and $\boldsymbol{u} \in V$ which satisfy $\boldsymbol{\Sigma} \in \mathcal{K}$, $\boldsymbol{u} \in \mathcal{C}$ and

$$\left.\begin{aligned} (A\boldsymbol{\Sigma},\, \boldsymbol{T}-\boldsymbol{\Sigma})_{S^2} - (\tilde{\boldsymbol{\varepsilon}}(\boldsymbol{u}),\, \boldsymbol{T}-\boldsymbol{\Sigma})_{S^2} &\geq 0 && \forall\, \boldsymbol{T} \in \mathcal{K} \\ -(\operatorname{div} \boldsymbol{\Sigma},\, \boldsymbol{v}-\boldsymbol{u})_{L^2(\Omega;\mathbb{R}^3)} &\geq (\boldsymbol{f},\, \boldsymbol{v}-\boldsymbol{u})_{L^2(\Omega;\mathbb{R}^3)} && \forall\, \boldsymbol{v} \in \mathcal{C}. \end{aligned}\right\} \qquad (\textbf{VIS})$$

The first variational inequality models the elastoplastic material behavior, while the second one takes the contact conditions into account. The variable $\boldsymbol{\Sigma}$ denotes the couple of generalized stresses $(\boldsymbol{\sigma}, \boldsymbol{\chi})$, where $\boldsymbol{\sigma}$ is the Cauchy

Key words and phrases. adaptivity, finite elements, optimal control.

stress tensor and $\boldsymbol{\chi}$ is an internal variable modeling hardening. The associated displacement field is denoted by $\boldsymbol{u}$ and the applied volume force by $\boldsymbol{f}$. The domain occupied by the body in both the deformed and undeformed states is denoted by Ω. Its boundary Γ has $C^{0,1}$-regularity and consists of three disjoint parts, the Dirichlet boundary Γ_D, the Neumann boundary Γ_N and the contact boundary Γ_C, such that $\Gamma = \Gamma_D \cup \Gamma_N \cup \Gamma_C$. While Γ_D is a closed subset of Γ with positive measure, Γ_C satisfies $\Gamma_C \subset \Gamma \setminus \Gamma_D$, $\overline{\Gamma}_C \subsetneq \Gamma \subset \Gamma_D$. The underlying spaces and sets are defined by

$$\begin{aligned} S &:= L^2\big(\Omega; \mathbb{R}^{3\times 3}_{\mathrm{sym}}\big) \\ V &:= \big\{\boldsymbol{v} \in H^1\big(\Omega;\mathbb{R}^3\big) \colon \boldsymbol{v}(x) = 0 \text{ a.e. on } \Gamma_D\big\} \\ \mathcal{K} &:= \big\{\boldsymbol{\Sigma} \in S^2 : \phi(\boldsymbol{\Sigma}) \le 0 \text{ a.e. in } \Omega\big\} \\ \mathcal{C} &:= \big\{\boldsymbol{v} \in V : \boldsymbol{\tau_\nu} \boldsymbol{v}(x) \le g(x) \text{ a.e. on } \Gamma_C\big\}. \end{aligned}$$

We restrict our model to the von Mises yield condition with yield function

$$\phi(\boldsymbol{\Sigma}) = \frac{1}{2}\big(\|\boldsymbol{\sigma}^D + \boldsymbol{\chi}^D\|^2_{\mathbb{R}^{3\times 3}} - \tilde{\sigma}_0^2\big),$$

where $\tilde{\sigma}_0 > 0$ is the yield stress. Further we denote by $\boldsymbol{\tau_\nu} \boldsymbol{v}(x) = \boldsymbol{\nu}(x) \cdot \boldsymbol{v}(x)$ the normal trace with normal vector field $\boldsymbol{\nu}$. The distance between work-piece and obstacle is given by the gap function $g\colon \mathbb{R}^2 \to \mathbb{R}$,

$$g = \frac{\psi - \varphi}{\sqrt{1 + \nabla\varphi^T \nabla\varphi}}.$$

Here ψ and ϕ are parametrizations of the obstacle and the contact boundary, respectively. For $\boldsymbol{\Sigma} = (\boldsymbol{\sigma}, \boldsymbol{\chi}) \in S^2$ and $\boldsymbol{T} = (\boldsymbol{\tau}, \boldsymbol{\mu}) \in S^2$, the operator A is defined through

$$(A\boldsymbol{\Sigma},\, \boldsymbol{T}) = \int_\Omega \boldsymbol{\tau} : \mathbb{C}^{-1}\boldsymbol{\sigma}\, \mathrm{d}x + \int_\Omega \boldsymbol{\mu} : \mathbb{H}^{-1}\boldsymbol{\chi}\, \mathrm{d}x$$

with compliance tensor

$$\mathbb{C}^{-1}\boldsymbol{\sigma} = \frac{1}{2\,\mu}\boldsymbol{\sigma} - \frac{\lambda}{2\,\mu\,(2\,\mu + 3\,\lambda)} \operatorname{trace}(\boldsymbol{\sigma})\mathbb{1}$$

and hardening modulus $\mathbb{H}^{-1}\boldsymbol{\chi} = \boldsymbol{\chi}/k_1$. The parameters λ, μ and k_1 are the Lamé constants and the hardening constant, respectively. Moreover, $\operatorname{div}\boldsymbol{\Sigma} = \operatorname{div}\boldsymbol{\sigma}$ is the divergence operator and $\tilde{\boldsymbol{\varepsilon}}\colon V \to S^2$ is given by

$$\tilde{\boldsymbol{\varepsilon}}(\boldsymbol{u}) = \begin{pmatrix} \boldsymbol{\varepsilon}(\boldsymbol{u}) \\ 0 \end{pmatrix},$$

where $\boldsymbol{\varepsilon}(\boldsymbol{u}) = \frac{1}{2}\big(\nabla\boldsymbol{u} + (\nabla\boldsymbol{u})^T\big)$ is the (linearized) strain tensor.

3 Optimization

We aim to minimize a tracking-type functional for the displacement $\boldsymbol{u}$ with a Tikhonov-term for the force $\boldsymbol{f}$ under the constraint (**VIS**). Introducing the Operator $F\colon S \to S$, defined by

$$\boldsymbol{F}(\boldsymbol{\tau}) = (2\mu + 3\lambda)\boldsymbol{\tau}^S + 2\mu\boldsymbol{\tau}^D - \frac{2\mu}{k_1 + 2\mu} \max\left(0, 2\mu - \frac{\tilde{\sigma}_0}{\|\boldsymbol{\tau}^D\|_{\mathbb{R}^{3\times 3}}}\right)\boldsymbol{\tau}^D,$$

we can reduce (**VIS**) to one variational inequality formulated only in the displacement, c.f. [6]. To be more precise, we obtain

$$-\left(\operatorname{div}\boldsymbol{F}(\boldsymbol{\varepsilon}(\boldsymbol{u})),\, \boldsymbol{v} - \boldsymbol{u}\right)_{L^2(\Omega;\mathbb{R}^3)} \ge (\boldsymbol{f},\, \boldsymbol{v} - \boldsymbol{u})_{L^2(\Omega;\mathbb{R}^3)} \quad \forall\, \boldsymbol{v} \in \mathcal{C}. \tag{VI}$$

The optimization problem under consideration then reads

$$\left.\begin{aligned} \text{Minimize} \quad & J(\boldsymbol{u}, \boldsymbol{f}) := \frac{1}{2}\,\|\boldsymbol{u} - \boldsymbol{u}_d\|^2_{L^2(\Omega;\mathbb{R}^3)} + \frac{\alpha}{2}\,\|\boldsymbol{f}\|^2_{L^2(\Omega;\mathbb{R}^3)} \\ \text{s.t.} \quad & \text{the elastoplastic contact problem (}\mathbf{VI}\text{)} \end{aligned}\right\} \tag{P}$$

with Tikhonov parameter $\alpha > 0$.

3.1. Regularization. Since the solution operator of the constraint in (**P**) is not differentiable, we regularize (**VI**) in order to apply derivative-based optimization algorithms. This is done by two steps. First, the operator $\boldsymbol{F}$ in (**VI**) is replaced by a locally smoothed version $\boldsymbol{F}_\gamma$, defined by

$$\boldsymbol{F}_\gamma(\boldsymbol{\tau}) = (2\mu + 3\lambda)\boldsymbol{\tau}^S + 2\mu\boldsymbol{\tau}^D - \frac{2\mu}{k_1 + 2\mu}\max\nolimits_\gamma\left(2\mu - \frac{\sigma_0}{\|\boldsymbol{\tau}^D\|_{\mathbb{R}^{3\times3}}}\right)\boldsymbol{\tau}^D$$

with regularization parameter $\gamma > 0$. The Function $\max_\gamma$ is a C^2-approximation of $\max(0, x)$ constructed by

$$\max\nolimits_\gamma(x) = \begin{cases} 0, & x < -\gamma \\ \frac{3}{16}\gamma + \frac{1}{2}x + \frac{3}{8\gamma}x^2 - \frac{1}{16\gamma^3}x^4, & x \in [-\gamma, \gamma] \\ x, & x > \gamma. \end{cases}$$

Moreover we apply a bi-quadratic penalization technique to (**VI**). For this purpose we introduce the abbreviation $\boldsymbol{G}_\rho(\boldsymbol{u}_{\gamma\rho}) := \max\left(0, (\boldsymbol{\tau_\nu}\boldsymbol{u}_{\gamma\rho} - g)/\rho\right)^3$ with penalization parameter $\rho > 0$ and we end up with

$$-\int_\Omega \operatorname{div}\boldsymbol{F}_\gamma(\boldsymbol{\varepsilon}(\boldsymbol{u}_{\gamma\rho}))\cdot\boldsymbol{v}\,\mathrm{d}x + \int_{\Gamma_C}\boldsymbol{G}_\rho(\boldsymbol{u}_{\gamma\rho})\cdot\boldsymbol{\tau_\nu}\boldsymbol{v}\,\mathrm{d}s = \int_\Omega \boldsymbol{f}_{\gamma\rho}\cdot\boldsymbol{v}\,\mathrm{d}x \quad \forall\,\boldsymbol{v}\in V. \tag{$\mathbf{VI}_{\gamma\rho}$}$$

The regularized optimization problem consequently becomes

$$\left.\begin{array}{rl} \text{Minimize} & J(\boldsymbol{u}_{\gamma\rho}, \boldsymbol{f}_{\gamma\rho}) \\ \text{s.t.} & (\mathbf{VI}_{\gamma\rho}). \end{array}\right\} \tag{$\mathbf{P}_{\gamma\rho}$}$$

By construction the solution operator of ($\mathbf{VI}_{\gamma\rho}$) is twice continuously differentiable. We introduce the adjoint state $\boldsymbol{p}_{\gamma\rho} \in V$ as the solution of

$$-\int_\Omega \operatorname{div}\left(\boldsymbol{F}'_\gamma(\boldsymbol{\varepsilon}(\boldsymbol{u}_{\gamma\rho}))\boldsymbol{\varepsilon}(\boldsymbol{p}_{\gamma\rho})\right)\cdot\boldsymbol{v}\,\mathrm{d}x + \rho\int_{\Gamma_C}\boldsymbol{G}'_\rho(\boldsymbol{u}_{\gamma\rho})\boldsymbol{p}_{\gamma\rho}\cdot\boldsymbol{\tau_\nu}\boldsymbol{v}\,\mathrm{d}s = \int_\Omega(\boldsymbol{u}_{\gamma\rho} - \boldsymbol{u}_d)\cdot\boldsymbol{v}\,\mathrm{d}x \quad \forall\,\boldsymbol{v}\in V, \tag{$\mathbf{AVI}_{\gamma\rho}$}$$

where the derivative $\boldsymbol{F}'_\gamma$ is given by

$$\begin{aligned}\boldsymbol{F}'_\gamma(\boldsymbol{\tau})\delta\boldsymbol{\tau} = (2\mu + 3\lambda)\delta\boldsymbol{\tau}^S + 2\mu\delta\boldsymbol{\tau}^D - \frac{2\mu}{k_1 + 2\mu}\max\nolimits'_\gamma\left(\frac{1}{\alpha_2} - \frac{\sigma_0}{\|\boldsymbol{\tau}^D\|_{\mathbb{R}^{3\times3}}}\right)\frac{\sigma_0}{\|\boldsymbol{\tau}^D\|^3_{\mathbb{R}^{3\times3}}}\boldsymbol{\tau}^D\left(\boldsymbol{\tau}^D : \delta\boldsymbol{\tau}^D\right) \\ - \frac{2\mu}{k_1 + 2\mu}\max\nolimits_\gamma\left(\frac{1}{\alpha_2} - \frac{\sigma_0}{\|\boldsymbol{\tau}^D\|_{\mathbb{R}^{3\times3}}}\right)\delta\boldsymbol{\tau}^D.\end{aligned}$$

By standard arguments we arrive at the following optimality system for ($\mathbf{P}_{\gamma\rho}$)

$$\left.\begin{array}{l} (\mathbf{VI}_{\gamma\rho}) \\ (\mathbf{AVI}_{\gamma\rho}) \\ \boldsymbol{p}_{\gamma\rho} + \alpha\boldsymbol{f}_{\gamma\rho} = 0 \quad \text{a.e. in } \Omega. \end{array}\right\} \tag{$\mathbf{OS}_{\gamma\rho}$}$$

3.2. FE-Discretization. We discretize the optimality system ($\mathbf{OS}_{\gamma\rho}$) by a standard hexahedral triangulation of the domain Ω, where we allow one hanging node per facet. Furthermore the triangulation needs to have patch structure in order to evaluate the a posteriori error estimate. This property is illustrated in Figure 1. To be more precise, we replace V by the finite element space

$$V_h = \{\boldsymbol{v}_h \in V \colon v_h|_T \in Q_1(T)\ \forall T \in \mathcal{T}_h\},$$

where $Q_1(T)$ is the space of trilinear functions on the hexaeder T and $\mathcal{T}_h$ is a triangulation of Ω depending on the discretization parameter h. This leads to the regularized and discretized optimality system

$$\left.\begin{array}{l} (\mathbf{VI}^h_{\gamma\rho}) \\ (\mathbf{AVI}^h_{\gamma\rho}) \\ \boldsymbol{p}^h_{\gamma\rho} + \alpha\boldsymbol{f}^h_{\gamma\rho} = 0 \quad \text{a.e. in } \Omega. \end{array}\right\} \tag{$\mathbf{OS}^h_{\gamma\rho}$}$$

This system can be solved by Newton's method leading to a numerical solution $\left(\tilde{\boldsymbol{u}}^h_{\gamma\rho}, \tilde{\boldsymbol{p}}^h_{\gamma\rho}, \tilde{\boldsymbol{f}}^h_{\gamma\rho}\right)$, see Section 5.

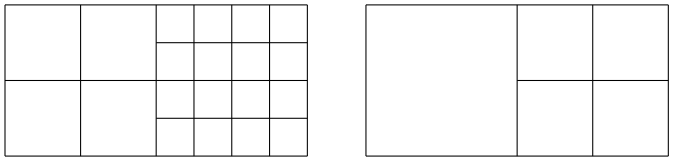

(a) Mesh with patch structure (b) Corresponding patch mesh

FIGURE 1. Illustration of the patch structure of the finite element mesh

4 A posteriori error estimation

Due to the regularization and discretization we performed in the last section the solution of $(\mathbf{OS}^h_{\gamma\rho})$ differs from the solution of the original optimization problem $(\mathbf{P})$. In total our solution involves a regularization error, a discretization error and a numerical error

$$\begin{aligned} J(\boldsymbol{u},\boldsymbol{f}) - J(\tilde{\boldsymbol{u}}^h_{\gamma,\rho},\tilde{\boldsymbol{f}}^h_{\gamma,\rho}) =& \underbrace{J(\boldsymbol{u},\boldsymbol{f}) - J(\boldsymbol{u}_{\gamma,\rho},\boldsymbol{f}_{\gamma,\rho})}_{\approx\eta_{\rho,\gamma}} + \underbrace{J(\boldsymbol{u}_{\gamma,\rho},\boldsymbol{f}_{\gamma,\rho}) - J(\tilde{\boldsymbol{u}}^h_{\gamma,\rho},\tilde{\boldsymbol{f}}^h_{\gamma,\rho})}_{\approx\eta_h+\eta_m} \\ \approx& \eta_{\rho,\gamma} + \eta_h + \eta_m. \end{aligned} \tag{4.1}$$

This section is dedicated to the estimation of the different errors by estimators $\eta_{\rho,\gamma}$, η_h, and η_m.

4.1. Discretization and Numerical Error. We handle the discretization error at the same time as the numerical error by applying the dual weighted residual method. In view of $\mathbf{VI}_{\gamma\rho}$, we introduce the operator $\mathcal{A} : V \times L^2\left(\Omega;\mathbb{R}^3\right) \times V \to \mathbb{R}$ given by

$$\mathcal{A}(\boldsymbol{u})(\boldsymbol{f},\boldsymbol{v}) := -\int_\Omega \operatorname{div} \boldsymbol{F}_\gamma(\boldsymbol{\varepsilon}(\boldsymbol{u}_{\gamma\rho}))\cdot\boldsymbol{v}\,\mathrm{d}x + \int_{\Gamma_C} \boldsymbol{G}_\rho(\boldsymbol{u}_{\gamma\rho})\cdot\boldsymbol{\tau_\nu}\boldsymbol{v}\,\mathrm{d}s - \int_\Omega \boldsymbol{f}_{\gamma\rho}\cdot\boldsymbol{v}\,\mathrm{d}x.$$

In the error estimate, we use the dual residuum

$$\tilde{\rho}^*(\cdot) := J'_{\boldsymbol{u}}(\tilde{\boldsymbol{u}}^h_{\gamma,\rho},\tilde{\boldsymbol{f}}^h_{\gamma,\rho})(\cdot) - \mathcal{A}'_{\boldsymbol{u}}(\tilde{\boldsymbol{u}}^h_{\gamma,\rho})(\tilde{\boldsymbol{f}}^h_{\gamma,\rho},\cdot,\tilde{\boldsymbol{p}}^h_{\gamma,\rho}),$$

the control residuum

$$\tilde{\rho}^{\boldsymbol{f}}(\cdot) := J'_{\boldsymbol{f}}(\tilde{\boldsymbol{u}}^h_{\gamma,\rho},\tilde{\boldsymbol{f}}^h_{\gamma,\rho})(\cdot) - \mathcal{A}'_{\boldsymbol{f}}(\tilde{\boldsymbol{u}}^h_{\gamma,\rho})(\tilde{\boldsymbol{f}}^h_{\gamma,\rho},\cdot,\tilde{\boldsymbol{p}}^h_{\gamma,\rho}),$$

and the primal residuum

$$\tilde{\rho}(\cdot) := -\mathcal{A}(\tilde{\boldsymbol{u}}^h_{\gamma,\rho})(\tilde{\boldsymbol{f}}^h_{\gamma,\rho},\cdot).$$

From [18] , we obtain

$$\begin{aligned} J(\boldsymbol{u}_{\gamma,\rho},\boldsymbol{f}_{\gamma,\rho}) - J(\tilde{\boldsymbol{u}}^h_{\gamma,\rho},\tilde{\boldsymbol{f}}^h_{\gamma,\rho}) =& \frac{1}{2}\tilde{\rho}^*\left(\boldsymbol{u}_{\gamma,\rho} - \tilde{\boldsymbol{u}}^h_{\gamma,\rho}\right) + \frac{1}{2}\tilde{\rho}^{\boldsymbol{f}}\left(\boldsymbol{f}_{\gamma,\rho} - \tilde{\boldsymbol{f}}^h_{\gamma,\rho}\right) \\ &+ \frac{1}{2}\tilde{\rho}\left(\boldsymbol{p}_{\gamma,\rho} - \tilde{\boldsymbol{p}}^h_{\gamma,\rho}\right) - \tilde{\rho}\left(\tilde{\boldsymbol{p}}^h_{\gamma,\rho}\right) + \mathcal{R}_h \end{aligned}$$

with a higher order term $\mathcal{R}_h$ depending on the regularization parameters γ,ρ. The first three terms measure the discretization error, whereas the fourth measures the numerical error. Due to the fact that $\boldsymbol{u}_{\gamma,\rho}$ and $\boldsymbol{f}_{\gamma,\rho}$ are unknown, we cannot use the first terms directly. However, they can numerically be approximated by applying an appropriate higher order interpolation operator. We choose a triquadratic interpolation operator $I^{(2)}_{2h}$ operating on the patch structure. This operator satisfies

$$I\tilde{\boldsymbol{u}}^h_{\gamma,\rho} - \tilde{\boldsymbol{u}}^h_{\gamma,\rho} \approx \boldsymbol{u}_{\gamma,\rho} - \tilde{\boldsymbol{u}}^h_{\gamma,\rho}.$$

We define the numerical error estimator by

$$\eta_m := -\tilde{\rho}\left(\tilde{\boldsymbol{p}}^h_{\gamma,\rho}\right)$$

and the discretization error estimator by

$$\eta_h := \frac{1}{2}\tilde{\rho}^*\left(I^{(2)}_{2h}\tilde{\boldsymbol{u}}^h_{\gamma,\rho} - \tilde{\boldsymbol{u}}^h_{\gamma,\rho}\right) + \frac{1}{2}\tilde{\rho}^{\boldsymbol{f}}\left(I^{(2)}_{2h}\tilde{\boldsymbol{f}}^h_{\gamma,\rho} - \tilde{\boldsymbol{f}}^h_{\gamma,\rho}\right) + \frac{1}{2}\tilde{\rho}\left(I^{(2)}_{2h}\tilde{\boldsymbol{p}}^h_{\gamma,\rho} - \tilde{\boldsymbol{p}}^h_{\gamma,\rho}\right).$$

It follows

$$J(\boldsymbol{u}_{\gamma,\rho},\boldsymbol{f}_{\gamma,\rho}) - J(\tilde{\boldsymbol{u}}^h_{\gamma,\rho},\tilde{\boldsymbol{f}}^h_{\gamma,\rho}) \approx \eta_h + \eta_m.$$

4.2. Regularization error estimator. Equation (4.1) indicates that we want to estimate the regularization error on the basis of the term

$$J(\boldsymbol{u}, \boldsymbol{f}) - J(\boldsymbol{u}_{\gamma,\rho}, \boldsymbol{f}_{\gamma,\rho}).$$

However, this approach conceals the fact that we have to develop an estimator for the error caused by the regularization with respect to the contact on the one hand and for the regularization error introduced by the hardening model on the other hand.

We estimate both terms using the same technique and discuss the applied approach in detail only for the contact regularization. The basic idea is that a second solution for an improved regularization parameter is calculated and the error is then estimated by the difference of the linear extrapolated value of the objective functional on the basis of the improved and the current value as well as of the current value, see equations (4.2)-(4.5). For efficient extrapolation, it is assumed here that

$$|J(\boldsymbol{u}, \boldsymbol{f}) - J(\boldsymbol{u}_{\rho}, \boldsymbol{f}_{\rho})| \leq C\rho^{-1} + HOT$$

holds. This has been proven for obstacle problems in [18].

For that purpose we take the objective functional J at $(\boldsymbol{u}_\rho, \boldsymbol{f}_\rho)$ as a function $\tilde{J}(\cdot)$ depending on ρ. Using the points $(\rho, \tilde{J}(\rho))$ and $(c\rho, \tilde{J}(c\rho))$ in $\mathbb{R} \times \mathbb{R}$ with a constant factor $0 < c < 1$ we create a straight line given by

$$f(x) = \frac{x - \rho}{c\rho - \rho}\tilde{J}(c\rho) + \frac{x - c\rho}{\rho - c\rho}\tilde{J}(\rho).$$

The value in 0 leads to the extrapolated point $(0, \tilde{J}_\infty)$,

$$\tilde{J}_\infty := \frac{1}{1-c}\left(\tilde{J}(c\rho) - \tilde{J}(\rho)\right) = f(0).$$

This linear extrapolation equals the first extrapolation step in the scheme of Neville and Aitken, see [9, p.318].

The same problem as in section 4.1 occurs. We only get an approximation $(\tilde{\boldsymbol{u}}^h_{\gamma,\rho}, \tilde{\boldsymbol{f}}^h_{\gamma,\rho})$ of the regularized and discretized solution. Here, we simply replace the analytical values by the discrete ones and define

$$J_{\gamma,\infty} := \frac{1}{1-c}\left(J(\tilde{\boldsymbol{u}}^h_{c\gamma,\rho}, \tilde{\boldsymbol{f}}^h_{c\gamma,\rho}) - J(\tilde{\boldsymbol{u}}^h_{\gamma,\rho}, \tilde{\boldsymbol{f}}^h_{\gamma,\rho})\right), \tag{4.2}$$

$$J_{\rho,\infty} := \frac{1}{1-c}\left(J(\tilde{\boldsymbol{u}}^h_{\gamma,c\rho}, \tilde{\boldsymbol{f}}^h_{\gamma,c\rho}) - J(\tilde{\boldsymbol{u}}^h_{\gamma,\rho}, \tilde{\boldsymbol{f}}^h_{\gamma,\rho})\right), \tag{4.3}$$

as well as the regularization error estimators

$$\eta_\gamma := J_{\gamma,\infty} - J(\tilde{\boldsymbol{u}}^h_{\gamma,\rho}, \tilde{\boldsymbol{f}}^h_{\gamma,\rho}) = \frac{1}{1-c}\left(J(\tilde{\boldsymbol{u}}^h_{c\gamma,\rho}, \tilde{\boldsymbol{f}}^h_{c\gamma,\rho}) - (2-c)J(\tilde{\boldsymbol{u}}^h_{\gamma,\rho}, \tilde{\boldsymbol{f}}^h_{\gamma,\rho})\right) \tag{4.4}$$

and

$$\eta_\rho := J_{\rho,\infty} - J(\tilde{\boldsymbol{u}}^h_{\gamma,\rho}, \tilde{\boldsymbol{f}}^h_{\gamma,\rho}) = \frac{1}{1-c}\left(J(\tilde{\boldsymbol{u}}^h_{\gamma,c\rho}, \tilde{\boldsymbol{f}}^h_{\gamma,c\rho}) - (2-c)J(\tilde{\boldsymbol{u}}^h_{\gamma,\rho}, \tilde{\boldsymbol{f}}^h_{\gamma,\rho})\right). \tag{4.5}$$

Using equations (4.2)-(4.5), we receive

$$\begin{aligned} J(\boldsymbol{u}, \boldsymbol{f}) - J(\tilde{\boldsymbol{u}}^h_{\gamma,\rho}, \tilde{\boldsymbol{f}}^h_{\gamma,\rho}) =& J(\boldsymbol{u}, \boldsymbol{f}) - J(\boldsymbol{u}_\rho, \boldsymbol{f}_\rho) + J(\boldsymbol{u}_\rho, \boldsymbol{f}_\rho) - J(\boldsymbol{u}_{\gamma,\rho}, \boldsymbol{f}_{\gamma,\rho}) \\ &+ J(\boldsymbol{u}_{\gamma,\rho}, \boldsymbol{f}_{\gamma,\rho}) - J(\tilde{\boldsymbol{u}}^h_{\gamma,\rho}, \tilde{\boldsymbol{f}}^h_{\gamma,\rho}) \\ \approx& \eta_\rho + \eta_\gamma + \eta_h + \eta_m. \end{aligned}$$

This is the rationale behind defining the global error estimator

$$\eta := \eta_\rho + \eta_\gamma + \eta_h + \eta_m.$$

5 Adaptive solution algorithm

In this section, we will discuss the adaptive solution algorithm. The main goal is to reduce efficiently the value of the total error measured by η. In order to achieve this at comparatively low computational costs, we also aim to balance the different error estimators. It is advised against decreasing solely one error estimator first, while the other estimators remain bigger, because the total estimator would not decrease efficiently. Yet, the numerical error estimate should always be smaller than the other error estimates to prevent numerical pollution effects. Therefore, we introduce a constant safety factor $\varkappa = 0.01$, cf. [18], and a constant equilibration factor $\epsilon > 1$, e.g. $\epsilon = 5$.

Algorithm 5.1. *Let $l = 0$ be the iteration index, $tol > 0$ some small tolerance, γ the initial regularization parameter for the regularized hardening model and ρ the initial regularization parameter for the contact regularization, then perform the following steps.*

(1) *Compute an approximation of the twice regularized and discretized solution* $(\tilde{\boldsymbol{u}}^h_{\gamma,\rho}, \tilde{\boldsymbol{f}}^h_{\gamma,\rho})$ *by applying the globalized Newton's method and start with the* numerical adaptivity*.*
   (a) *Perform Newton steps, until the method does not damp anymore.*
   (b) *Use the DWR method to estimate the numerical and the discretization error with* η_m *and* η_h*.*
   (c) *While* $|\eta_m| \geq \varkappa \cdot |\eta_h|$*, do another Newton step (*numerical adaptivity*). In reality, we do not perform only one additional Newton step, but two or three without estimating the DWR estimator in between due to the cost of that estimation.*

(2) *Now that the numerical pollution is not dominating, estimate the regularization error.*
   (a) *Use Newton's method to calculate the auxiliary solution* $(\tilde{\boldsymbol{u}}^h_{c\gamma,\rho}, \tilde{\boldsymbol{f}}^h_{c\gamma,\rho})$*.*
   (b) *Compute* η_ρ*.*
   (c) *Use Newton's method to calculate the auxiliary solution* $(\tilde{\boldsymbol{u}}^h_{c\gamma,\rho}, \tilde{\boldsymbol{f}}^h_{c\gamma,\rho})$*.*
   (d) *Compute* η_γ*.*

(3) *If* $\eta \leq tol$*, then stop.*

(4) *Adaptively modify the discretization or the regularization.*

(5) *Set* $l = l + 1$ *and return to (1).*

Step (4) is now outlined in more detail. We call an error estimator η_i dominating, if $\eta_i > \epsilon\, \eta_j$ for all $j \neq i$ and the equilibration factor ϵ. The step (1c) of algorithm 5.1 ensures that the numerical error will not dominate the total error. Each one of the remaining three estimates can be the crucial part of our estimator - on its own or in combination with one or two other estimates. I.e. we have to treat 2^3 cases in the balacing method. Due to this large number, the details of step (4) in the algorithm 5.1 are not shown, but it is outlined how to take action for only one dominating part.

(1) In case of a dominating discretization error estimator, we localize the error estimator and perform a classic $h-$adaptive mesh refinement. The localization is done by filtering as seen in [8].

(2) In case of a dominating regularization error estimator, we decrease either ρ or γ by multiplying a constant factor $0 < c < 1$. One might consider a more sophisticated approach. Depending on the number of Newton steps in step (4), the factor c should change. If the number of Newton steps is large, then c should be closer to one.

6 Numerical results

In this section, we consider two numerical examples in order to test our numerical algorithm. The first one only includes elasto-plastic material behavior and illustrates the need for path following and regularization. The second one is a three dimensional elasto-plastic contact problem, which is motivated by the incrementel rolling process.

6.1. Elasto-plastic example. In this example, the objective functional tracks the state both on the entire domain and on a submanifold of the domain. The control cost is taken into account by a tracking type term as well. There are no constraints on the control, which acts in a distributed way on the domain. The Dirichlet boundary is the whole boundary of the domain. A locally optimal control is known, whose corresponding state has a biactive set with a positive measure. The computational domain is given by $\Omega = \{x \in \mathbb{R}^2 : \|x\| < 1\}$ with the two subdomains $B = \{x \in \mathbb{R}^2 \colon \|x\| < 1/2\}$ and $R = \Omega \setminus B$. The material constants are chosen as follows: hardening constant $k_1 = 1.0$, elasticity modulus $E = 1.0$, Poisson number $\nu = 0.0$, and the yield stress $\sigma_0 > 0$. The desired state in the domain is specified as

$$\boldsymbol{u}_\Omega = \begin{cases} \begin{pmatrix} U\left(\|x\|^2\right) + \left(8x_1^2 + 4x_2^2 + 4x_1x_2\right) U''\left(\|x\|^2\right) + 6U'\left(\|x\|^2\right) \\ U\left(\|x\|^2\right) + \left(4x_1^2 + 8x_2^2 + 4x_1x_2\right) U''\left(\|x\|^2\right) + 6U'\left(\|x\|^2\right) \end{pmatrix}, & x \in B, \\ \begin{pmatrix} U\left(\|x\|^2\right) + \left(6x_1^2 + 2x_2^2 + 4x_1x_2\right) U''\left(\|x\|^2\right) + 4U'\left(\|x\|^2\right) \\ U\left(\|x\|^2\right) + \left(2x_1^2 + 6x_2^2 + 4x_1x_2\right) U''\left(\|x\|^2\right) + 4U'\left(\|x\|^2\right) \end{pmatrix}, & x \in R, \end{cases}$$

with

$$U(t) = \begin{cases} -\sigma_0 t^2 + \frac{3}{2}\sigma_0 t - \frac{13}{16}\sigma_0, & t < \frac{1}{4}, \\ \sigma_0\sqrt{t} - \sigma_0, & t \geq \frac{1}{4}. \end{cases}$$

As desired state on the submanifold ∂B, we choose

$$\boldsymbol{u}_{\partial B} = \begin{pmatrix} -\sigma_0 \\ -\sigma_0 \end{pmatrix}.$$

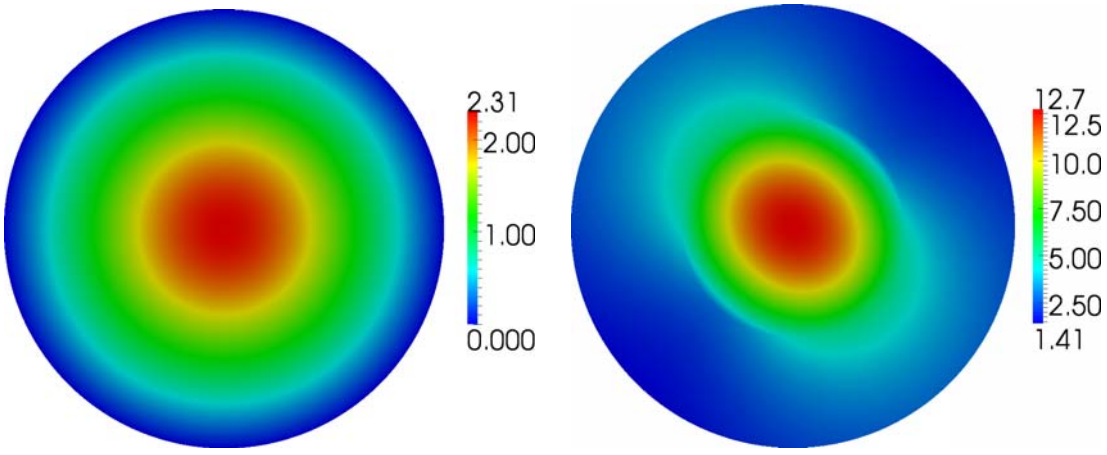

(a) Analytical optimal state $|\bar{\boldsymbol{u}}|$ (b) Analytical optimal control $|\bar{\boldsymbol{f}}|$

FIGURE 2. Illustration of the analytical solution of the elasto-plastic example

The desired control is given by

$$\boldsymbol{f}_\Omega = \begin{pmatrix} \frac{2}{\alpha} U\left(\|x\|^2_{\mathbb{R}^2}\right) - \left(4x_1^2 + 2x_2^2 + 2x_1x_2\right) U''\left(\|x\|^2_{\mathbb{R}^2}\right) - 3U'\left(\|x\|^2_{\mathbb{R}^2}\right) \\ \frac{2}{\alpha} U\left(\|x\|^2_{\mathbb{R}^2}\right) - \left(2x_1^2 + 4x_2^2 + 2x_1x_2\right) U''\left(\|x\|^2_{\mathbb{R}^2}\right) - 3U'\left(\|x\|^2_{\mathbb{R}^2}\right) \end{pmatrix}, \quad \alpha > 0.$$

A local optimal control and state are known analytically. By

$$\boldsymbol{f} = -\operatorname{div}(\boldsymbol{\varepsilon}(\boldsymbol{u}))$$

a local optimal control is given with the optimal state

$$\boldsymbol{u} = \begin{pmatrix} U\left(\|x\|^2_{\mathbb{R}^2}\right) \\ U\left(\|x\|^2_{\mathbb{R}^2}\right) \end{pmatrix},$$

as well as $\boldsymbol{\sigma} = \boldsymbol{\varepsilon}(\boldsymbol{u})$ and $\boldsymbol{\chi} = \boldsymbol{0}$. The optimal control and state is illustrated in Figure 2.

Since we know the analytical solution $(\bar{\boldsymbol{u}}, \bar{\boldsymbol{f}})$, we can derive the exact goal value

$$J(\bar{\boldsymbol{u}}, \bar{sv}) \approx 156.44873847926598083.$$

We are going to use this value in order to analyse the difference between the value of the approximated solution of the regularized and discretized problem and the exact goal value for no regularization and no discretization.

For that purpose we define

$$E_D := \frac{J(\bar{\boldsymbol{u}}, \bar{\boldsymbol{f}}) - \tilde{J}(\tilde{\boldsymbol{u}}^h_\gamma, \tilde{\boldsymbol{f}}^h_\gamma)}{J(\bar{\boldsymbol{u}}, \bar{\boldsymbol{f}})},$$

where $\tilde{J}$ denotes the usage of a quadrature functional Q. Also, we apply this quadrature to the difference between the analytical $(\bar{\boldsymbol{u}}, \bar{\boldsymbol{f}})$ and the numerical solution $(\tilde{\boldsymbol{u}}^h_\gamma, \tilde{\boldsymbol{f}}^h_\gamma)$, which leads to

$$\|\cdot\|_{Q;2} \approx \|\cdot\|_{L^2}$$

The adaptive solution algorithm 5.1 involves a path following approach for the reduction of the regularization parameters γ and ρ based on a fixed reduction factor c starting from initial guesses γ_0 and ρ_0. Here, we study the dependence of the solution algorithm on the reduction factor c and the initial regularization factors γ_0 and ρ_0. To simplify the presentation we only consider the elasto-plastic example without contact on a fixed mesh with 4672 elements. In Figure 3 the developement of the residuum in Newton's method ist depicted for different path following approaches, where the aim is to calculate a numerical solution to the regularization parameter $\gamma_a = 10^{-4}$. In the first approach we choose $\gamma_0 = \gamma_a$. However, Newton's method does not converge within 100 iterations, where very small damping parameters arise from the globalization method. The second idea is to start with a large $\gamma_0 = 0.125$ and reduce it in one step to $\gamma_0 \approx \gamma_a$ by a reduction factor of $c = 10^{-3}$. Here, we observe fast Newton like convergence for the nonlinear system with respect to γ_0 but no convergence in the second step of the path following algorithm. Using $\gamma_0 = 0.125$ and $c = 0.125$ the path following algorithm achieves a numerical solution for $\gamma = 0.125^5 < \gamma_a$ within a total number of 40 Newton steps, where we observe fast Newton like convergence in every step of the path following algorithm. This example substantiates the

need for the path following algorithm with a relatively large initial regularization parameter γ_0 and a moderate reduction factor c.

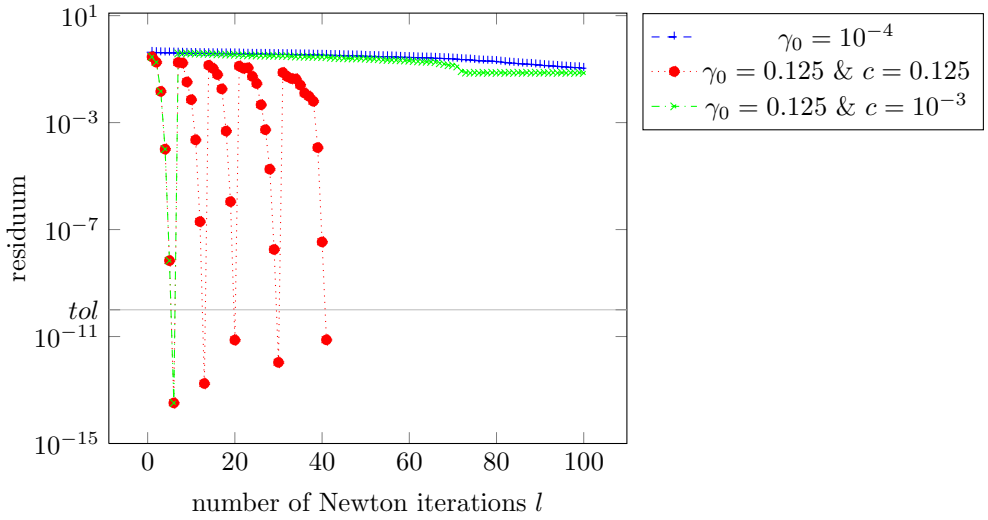

FIGURE 3. Developement of the residuum in Newton's method for different path following approaches on a mesh with 4672 elements

In Table 1, the results of the path following algorithm for a fixed mesh with 74, 752 elements and a comparatively small reduction factor $c = 0.125$ are presented. We find fast convergence for the Newton algorithm in the first steps and due to bad numerical conditioning a slower convergence in the last steps. However, in the last steps no error reduction is observed since the discretization error is dominating.

k	γ_k	E_D	$\|\bar{\boldsymbol{u}} - \tilde{\boldsymbol{u}}_\gamma^h\|_{Q;2}$	$\|\bar{\boldsymbol{f}} - \tilde{\boldsymbol{f}}_\gamma^h\|_{Q;2}$	# NEWTON-ITER.
0	$7.5000{\cdot}10^{-1}$	$-1.24269377{\cdot}10^{-2}$	$1.56518165{\cdot}10^{-1}$	$4.01601839{\cdot}10^{-1}$	4
1	$9.3750{\cdot}10^{-2}$	$-2.39870115{\cdot}10^{-3}$	$6.83487930{\cdot}10^{-2}$	$3.78258028{\cdot}10^{-1}$	5
2	$1.1719{\cdot}10^{-2}$	$-6.94489780{\cdot}10^{-4}$	$1.55450241{\cdot}10^{-2}$	$3.19163821{\cdot}10^{-1}$	8
3	$1.4648{\cdot}10^{-3}$	$-4.54581384{\cdot}10^{-4}$	$5.48383853{\cdot}10^{-3}$	$3.15664293{\cdot}10^{-1}$	9
4	$1.8311{\cdot}10^{-4}$	$-4.38267995{\cdot}10^{-4}$	$4.73682332{\cdot}10^{-3}$	$3.15633336{\cdot}10^{-1}$	7
5	$2.2888{\cdot}10^{-5}$	$-4.37098404{\cdot}10^{-4}$	$4.68354309{\cdot}10^{-3}$	$3.15627941{\cdot}10^{-1}$	10
6	$2.8610{\cdot}10^{-6}$	$-4.37036479{\cdot}10^{-4}$	$4.68058301{\cdot}10^{-3}$	$3.15629235{\cdot}10^{-1}$	11
7	$3.5763{\cdot}10^{-7}$	$-4.37030759{\cdot}10^{-4}$	$4.68029185{\cdot}10^{-3}$	$3.15629564{\cdot}10^{-1}$	22
8	$4.4703{\cdot}10^{-8}$	$-4.37030060{\cdot}10^{-4}$	$4.68025614{\cdot}10^{-3}$	$3.15629594{\cdot}10^{-1}$	47

TABLE 1. Results of the path following approach on a fixed mesh with 74, 752 elements and a reduction factor $c = 0.125$

The convergence of the results with respect to finite element discretization is depicted in Table 2. Here, we observe a convergence of order h in the objective functional, whereas the convergence in the state and especially in the control is much slower.

# REF.	# ELE.	E_D	$\|\bar{\boldsymbol{u}} - \tilde{\boldsymbol{u}}_\gamma^h\|_{Q;2}$	$\|\bar{\boldsymbol{f}} - \tilde{\boldsymbol{f}}_\gamma^h\|_{Q;2}$
1	1,168	$-3.30524393{\cdot}10^{-3}$	$1.97166366{\cdot}10^{-2}$	$8.72658009{\cdot}10^{-1}$
2	4,672	$-1.67781407{\cdot}10^{-3}$	$1.30081961{\cdot}10^{-2}$	$6.25448788{\cdot}10^{-1}$
3	18,688	$-8.48978498{\cdot}10^{-4}$	$7.69568226{\cdot}10^{-3}$	$4.45096035{\cdot}10^{-1}$
4	74,752	$-4.37825927{\cdot}10^{-4}$	$4.71645566{\cdot}10^{-3}$	$3.15632653{\cdot}10^{-1}$
5	299,008	$-2.22887604{\cdot}10^{-4}$	$2.64650995{\cdot}10^{-3}$	$2.23366448{\cdot}10^{-1}$

TABLE 2. Convergence of the results with respect to the mesh size for $\gamma = 1.3394 \cdot 10^{-4}$

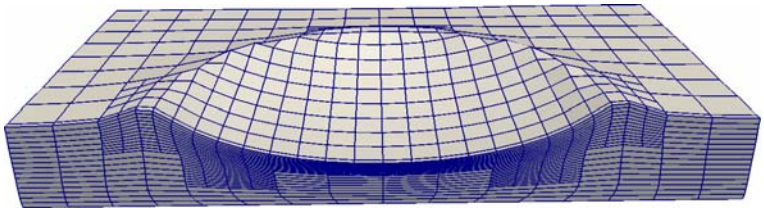

FIGURE 4. Adaptive mesh with 1 elements in the sixth iteration of the adpative algorithm

6.2. 3D elasto-plastic contact example. As second example we consider an elasto-plastic contact problem. Here, the computational domain is given by $\Omega = [0, 0.25] \times [-1, 1]^2$, where we assume homogeneous Dirichlet boundary conditions on $\Gamma_D = \{0\} \times [-1, 1]^2$. The possible contact boundary is given by $\Gamma_C = 0.25 \times [-1, 1]^2$. The material constants are chosen as follows: hardening constant $k_1 = 1.8$, elasticity modulus $E = 200.0$, Poisson number $\nu = 0.3$, and the yield stress $\sigma_0 = 10.0$. The obstacle is given by a sphere of radius 1 and midpoint $(1.125, 0, 0)$. The results of the adaptive algorithm are summarized in Table 3. Here, a fixed reduction rate of $c = (\sqrt[3]{10})^{-1}$ was used and the adaptive mesh refinement was based on a fixed fraction strategy refining the 5% of the cells with the largest error. Furthermore, the equilibration factor ϵ was chosen as 0.01 and the numerical safety factor $\varkappa$ as 0.001.We observe that the error with respect to the contact regularization is the dominant error source in the first iterations. With decreasing penalty parameter, the discretization error becomes more and more important. The regularization error with respect to the elasto-plastic material as wells as the numerical error is neglectable. The adaptive mesh in the sixth iteration is depicted in Figure 4, where mesh refinement is mainly carried out in the contact zone.

ITER.	# ELE,	ρ	γ	η_h	η_m	η_ρ	η_γ
0	512	$1.00000{\cdot}10^{-2}$	$1.0{\cdot}10^{-3}$	$9.82240{\cdot}10^{-6}$	$6.53217{\cdot}10^{-12}$	$1.06886{\cdot}10^{-4}$	$1.33257{\cdot}10^{-14}$
1	960	$4.64159{\cdot}10^{-3}$	$1.0{\cdot}10^{-3}$	$4.33174{\cdot}10^{-7}$	$5.05989{\cdot}10^{-11}$	$6.32937{\cdot}10^{-5}$	$1.46377{\cdot}10^{-12}$
2	960	$2.15443{\cdot}10^{-3}$	$1.0{\cdot}10^{-3}$	$2.12746{\cdot}10^{-6}$	$1.26724{\cdot}10^{-17}$	$3.32287{\cdot}10^{-5}$	$0.00000{\cdot}10^{0}$
3	1,576	$1.00000{\cdot}10^{-3}$	$1.0{\cdot}10^{-3}$	$5.17851{\cdot}10^{-6}$	$1.76127{\cdot}10^{-10}$	$1.63104{\cdot}10^{-5}$	$1.69732{\cdot}10^{-12}$
4	2,752	$4.64159{\cdot}10^{-4}$	$1.0{\cdot}10^{-3}$	$5.66032{\cdot}10^{-6}$	$2.92014{\cdot}10^{-10}$	$7.34226{\cdot}10^{-6}$	$8.51965{\cdot}10^{-13}$
5	5,440	$2.15443{\cdot}10^{-4}$	$1.0{\cdot}10^{-3}$	$4.05639{\cdot}10^{-6}$	$4.00698{\cdot}10^{-10}$	$3.66864{\cdot}10^{-6}$	$6.39670{\cdot}10^{-13}$
6	9,920	$1.00000{\cdot}10^{-4}$	$1.0{\cdot}10^{-3}$	$3.11739{\cdot}10^{-6}$	$3.93422{\cdot}10^{-10}$	$1.56246{\cdot}10^{-6}$	$1.99024{\cdot}10^{-13}$

TABLE 3. Results of the adaptive algorithm for the 3d example

7 Conclusion

We presented an adaptive algorithm for the optimal control of elasto-plastic deformation processes. The model includes static elasto-plasticity at small strains and geometric contact conditions. Both phenomena are modeled by VIs of the first kind. The optimal control of a mechanical system involving two VIs is the major genuine contribution of our work.

To cope with this challenge, we introduce two different regularizations which turn the coupled system of VIs into a nonlinear, but smooth PDE. The arising regularized optimal control problem is smooth and can thus be solved by standard Newton- or Newton-type methods. The regularized solutions are used as initial values for a subsequent iteration with updated regularization parameters. Therefore it does not make sense to solve these problems with a high numerical resolution. Instead regularization parameters and mesh size should be (locally) adapted such that regularization and discretization error are in balance. For this purpose estimators for all error contributions are needed. While the discretization error is estimated by means of the DWR method, we use an extrapolation technique for the two regularization errors, which requires to solve one additional regularized problem at each time the respective estimator is evaluated. Depending on which error contribution dominates, either the mesh is locally refined or the regularization parameters for the elasto-plastic material law or the contact conditions are updated.

This procedure allows to share a substantial amount of computing time, since most of the iterations in the optimization algorithm are performed on comparatively coarse meshes, as our numerical tests illustrate. In this way the algorithm is able to numerically solve the considered optimal control problem in a computational time that represents a small multitude of the computing time needed for the pure simulation.

To be able to tackle a real-world problem as the rolling of thermally coated surfaces, we first need to further accelerate the algorithm. To this end one has to develop a less costly estimator for the regularization error. A

technique, which performs the extrapolation using tangential information, has shown promising results for the optimal control of the obstacle problem, see [16]. Furthermore, one has to treat more involved models including all essential features of the rolling process such as finite strains or frictional contact. The latter will induce an additional VI of the second kind which will require a further regularization. This will be subject of future research.

References

[1] Bangerth, W. ; Rannacher, R. : *Adaptive finite element methods for differential equations*. Basel : Birkhäuser, 2003 (Lectures in Mathematics, ETH Zürich)

[2] Barbu, V. : *Research Notes in Mathematics*. Bd. 100: *Optimal Control of Variational Inequalities*. Boston : Pitman, 1984

[3] Becker, R. ; Rannacher, R. : A Feed-Back Approach to Error Control in Finite Element Methods: Basic Analysis and Examples. In: *East-West J. Numer. Math.* 4 (1996), S. 237–264

[4] Becker, R. ; Rannacher, R. : An optimal control approach to a posteriori error estimation in finite element methods. In: *Acta Numerica* 10 (2001), S. 1–102

[5] Bergounioux, M. : Use of augmented Lagrangian methods for the optimal control of obstacle problems. In: *Journal of Optimization Theory and Applications* 95 (1997), Nr. 1, S. 101–126

[6] Betz, T. : *Optimale Steuerung elastoplastischer Verformungsprozesse*. 2011. – Diplomarbeit, TU Darmstadt

[7] Betz, T. ; Meyer, C. : Second-Order Sufficient Optimality Conditions for Optimal Control of Static Elastoplasticity with Hardening. In: *ESAIM-COCV* (2014). – accepted

[8] Braack, M. ; Ern, A. : A posteriori control of modeling errors and discretization errors. In: *Multiscale Model. Simul.* 1 (2003), Nr. 2, S. 221–238. http://dx.doi.org/10.1137/S1540345902410482. – DOI 10.1137/S1540345902410482

[9] Deuflhard, P. ; Hohmann, A. : *Numerische Matheimatik 1 - Eine algorithmisch orientierte Einführung*. 4. Auflage. Berlin : De Gruyter, 2008

[10] Herzog, R. ; Meyer, C. ; Wachsmuth, G. : Integrability of Displacement and Stresses in Linear and Nonlinear Elasticity with Mixed Boundary Conditions. In: *Journal of Mathematical Analysis and Applications* 382 (2011), Nr. 2, S. 802–813. http://dx.doi.org/10.1016/j.jmaa.2011.04.074. – DOI 10.1016/j.jmaa.2011.04.074

[11] Hiegemann, L. ; Weddeling, C. ; Ben Khalifa, N. ; Tekkaya, A. : Control of the Matrial Flow in Deep Drawing by the Use of Rolled Surface Textures. In: *Proceeding of the sixth public colloquium of the SFB 708*, Verlag Praxiswissen, 2013

[12] Hintermüller, M. : Inverse Coefficient Problems for Variational Inequalities: Optimality Conditions and Numerical Realization. In: *ESAIM Mathematical Modelling and Numerical Analysis* 35 (2001), Nr. 1, S. 129–152

[13] Hintermüller, M. ; Kopacka, I. : Mathematical Programs with Complementarity Constraints in Function Space: C- and Strong Stationarity and a Path-Following Algorithm / Institute of Mathematics and Scientific Computing, University of Graz. 2008 (IFB-Report No. 11). – Forschungsbericht

[14] Ito, K. ; Kunisch, K. : Optimal Control of Elliptic Variational Inequalities. In: *Applied Mathematics and Optimization* 41 (2000), S. 343–364

[15] Kunisch, K. ; Wachsmuth, D. : Path-following for optimal control of stationary variational inequalities. In: *Computational Optimization and Applications* (2012), S. 1–29. http://dx.doi.org/10.1007/s10589-011-9400-8. – DOI 10.1007/s10589–011–9400–8

[16] Meyer, C. ; Rademacher, A. ; Wollner, W. : Adaptive optimal control of the obstacle problem / Fakultät für Mathematik, TU Dortmund. 2014. – Forschungsbericht. – Ergebnisberichte des Instituts für Angewandte Mathematik, Nummer 494

[17] Mignot, F. : Contrôle dans les inéquations variationelles elliptiques. In: *Journal of Functional Analysis* 22 (1976), Nr. 2, S. 130–185

[18] Rannacher, R. ; Vihharev, J. : Adaptive finite element analysis of nonlinear problems: balancing of discretization and iteration errors. In: *Journal of Numerical Mathematics* 21 (2013), Nr. 01, S. 23–62

[19] Schiela, A. ; Wachsmuth, D. : Convergence analysis of smoothing methods for optimal control of stationary variational inequalities / Johann Radon Institute for Computational and Applied Mathematics (RICAM). 2011 (2011-09). – Forschungsbericht

TU Dortmund, Faculty of Mathematics, Vogelpothsweg 87, D–44227 Dortmund, Germany

E-mail address: tbetz@math.tu-dortmund.de

E-mail address: cmeyer@math.tu-dortmund.de

E-mail address: andreas.rademacher@math.tu-dortmund.de

E-mail address: korinna.rosin@math.tu-dortmund.de